Vrije Universiteit Brussel

An improved Describing Function with applications for OTA-based circuits

Dries Peumans, *Student Member, IEEE* and Gerd Vandersteen, *Member, IEEE*

Abstract—**Electronic systems make extensive use of Operational Transconductance Amplifiers (OTA) to build filters and oscillators. Studying the effects of the saturation nonlinearity on these OTA-based circuits is difficult and often requires lengthy simulations to check the system's performance under large-signal operation. The Describing Function theory allows to circumvent these simulations by deriving a signal-dependent linearised gain, which predicts the effects of the nonlinearity. However, its use is limited since state-of-the-art Describing Functions deviate significantly from the real saturating behaviour of OTAs. This paper proposes an improved Describing Function which can be directly derived from the static nonlinear characteristic of the transconductance amplifier. The performance of the proposed methodology is demonstrated for both an OTA-based filter and oscillator. It is shown that the proposed describing function has a better nonlinear prediction capability than state-of-the-art solutions.**

Index Terms—**Describing Function theory, operational transconductance amplifier, oscillator.**

I. INTRODUCTION

Continuous-time active circuits using Operational Transconductance Amplifiers (OTA) and capacitors, also known as g_m-C circuits, have attracted the interest of designers due to their high-frequency capability (1 MHz - 100 MHz range), easy tunability and structural flexibility [1], [2]. However, in recent years, the CMOS downscaling has caused a substantial decline in the obtainable dynamic range (e.g. [3], [4] which propose new structures to cope with this decline). As a result, the OTA will behave nonlinearly whenever the linear signal range is exceeded. This nonlinear behaviour is a knife that cuts both ways: depending on the application at hand it is undesirable (e.g. creates distortion in filters) or unavoidable (e.g. to obtain high oscillation amplitudes in sinusoidal oscillators).

The general description of weakly nonlinear systems (Volterra) has been used in the past to predict the induced nonlinear effects within g_m-C filters [5], [6]. Although successful, this Volterra-based approach has one main disadvantage: interpretable results are obtained mainly for single-tone and two-tone excitations [7]. On the other hand, modern wireless communication systems have to deal with more complex digitally modulated signals, e.g. Orthogonal Frequency Domain Multiplexing (OFDM). The results obtained from the single-tone or two-tone case are therefore invalid due to the signal-dependent nonlinear nature of the OTA [8].

Another solid approach to describe nonlinear systems is based on the Describing Function (DF) theory [9]. The DF

D. Peumans and G.Vandersteen are with the Department of Fundamental Electricity and Instrumentation (ELEC), Vrije Universiteit Brussel (VUB), Pleinlaan 2, 1050 Brussels, Belgium.
E-mail: dries.peumans@vub.ac.be, gerd.vandersteen@vub.ac.be

approximates the input-output relationship of a static nonlinear block (including saturation and/or hysteresis phenomena) by a linear gain which is function of the excitation signal's characteristics (probability density function and power). By doing so, limit cycles can be studied in nonlinear autonomous systems (e.g. oscillators). Currently, realistic design flows merely use the DF to retrieve initial estimates of the system properties (i.e. oscillation frequency and amplitude). Obtaining an accurate representation proves impossible for most applications, due to the crude theoretical approximation that is used for the DF estimation.

Keeping the above mentioned issues in mind, we develop an improved DF which predicts the saturation behaviour for both single-tone and complex modulated excitations. More accurately, designers can then predict the effect of the saturation nonlinearity without the need to perform time-consuming simulations. Furthermore, the proposed DF is based on an approximating basis function which ensures that a proper model for the nonlinearity is obtained.

This paper is organised as follows: Section II proposes an approximating function which models static saturation behaviour better than the idealised one. Based on the proposed basis function, Section III derives the DF for both sinusoidal and Gaussian distributed signals and verifies the accuracy of the obtained DF with a more general test case. We conclude the paper by applying the derived DF on two examples in Section IV: a Tow-Thomas g_m-C biquad and a differential quadrature oscillator [10].

II. APPROXIMATION OF THE STATIC NONLINEAR BEHAVIOUR

In the past, the DF has proven to be helpful in a myriad of different applications. The DF allows to effectively analyse the nonlinear behaviour, estimate figures of merit such as gain compression and obtain information about system properties such as the presence of limit cycles ... without overcomplicating the mathematics involved [9]. The accuracy obtained depends heavily on two basic assumptions:

- the higher order harmonics generated by the nonlinear system are sufficiently attenuated by a linear filtering mechanism present in the system, and,
- the static nonlinear behaviour can be well approximated by a function for which the DF is computable.

The first assumption is directly related to the structure of the system at hand and cannot be easily circumvented without altering the system properties. Luckily, the second assumption gives some freedom to improve the accuracy of the DF by choosing an appropriate approximating analytic function of the static nonlinearity.
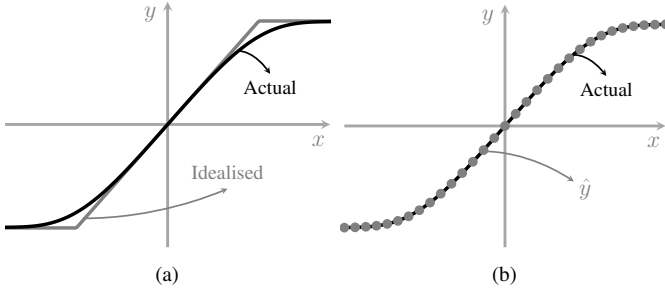
Fig. 1: (a) The generally used 'idealised' approximating function does not provide a good fit of the actual saturation behaviour. (b) The proposed approximation function in (1) provides a far more better fit ($R = 5$).

One commonly made approximation models the limiting behaviour of a saturation phenomenon by an abrupt change, while maintaining a perfectly linear operation in the intermediate region (see Fig. 1a) [9]. This highly idealised function is a widely used approximation, but cannot be applied in everyday practice due to the poor modelling power caused by its simplicity. Some bipolar transistor configurations (e.g. differential pair [11]) yield a $\tanh$ saturation characteristic [12] which is smooth and nevertheless allows for the numerical computation of the DF [13]. Unfortunately, this $\tanh$ function cannot be generally used to describe an arbitrary saturation behaviour.

To tackle these problems we propose to use the following approximating function instead

$$\hat{y}(x) = \sum_{n=0}^{R} \alpha_n \left(\frac{x}{\sqrt{1+x^2}} \right)^{2n+1} \qquad (1)$$

where x is the input control variable, $\hat{y}$ represents the approximated output variable of the saturation characteristic y, R is the order of the approximation and the α_n are the coefficients used for approximating y with $\hat{y}$ (they can be obtained with a linear least-squares regression). Only odd functions are added to $\hat{y}$ since the even terms result in a zero contribution when evaluating the DF [9].

The reason why we have chosen this function is two-fold: it is linear in the parameters α_n which allows to avoid potential costly nonlinear estimation difficulties and the small-signal linearised behaviour is easily defined by the coefficient α_0. Imposing that the modelled and simulated small-signal behaviour coincide is possible as

$$\lim_{x \to 0} \frac{\mathrm{d}\hat{y}}{\mathrm{d}x} = G_{SS} \quad \Rightarrow \quad \alpha_0 = G_{SS}$$

where G_{SS} is the small-signal gain obtained by linearising the actual system around its operating point. The estimation algorithm that is used is a traditional least-squares minimizer for all the coefficients α_n, except for α_0 which is fixed to G_{SS}.

The results of fitting $\hat{y}$ on the previously introduced saturation characteristic are illustrated for $R = 5$ in Fig. 1b. As it can be observed, $\hat{y}$ outperforms the idealised function in Fig. 1a (a relative error with respect to y of $-50\,\mathrm{dB}$ is obtained over the whole input range).

III. DESCRIBING FUNCTION ANALYSIS

The previous section dealt with the derivation of a model $\hat{y}$ which matches well the actual static nonlinear behaviour. An accurate approximation is essential since the DF will be applied to $\hat{y}$ instead of the actual saturation nonlinearity y.

Estimation of the DF is entirely based on the so-called quasi-linearisation technique [9], which approximates the nonlinear system by a linear time-invariant static gain that depends on both the power and shape of the input signal. This quasi-linearisation is applicable to any kind of input waveform, but the DF only considers three principal bases for its estimation: a constant bias, sinusoids and Gaussian distributed signals. We will restrict ourselves to the sinusoidal (see Section III-A) and Gaussian (see Section III-B) case, since they are the most interesting for the majority of applications. Also, removing the bias is justified because most electronic systems stabilise their operating point using dedicated circuitry (e.g. common-mode feedback).

Quasi-linearisation is based on finding the best linear static gain N_x which describes best, in least-squares sense, the nonlinear characteristic for the input signal $x(t)$. Minimising the variance of the approximation error e ($\mathbb{E}\{\bullet\}$ represents the expectation operator)

$$N_x = \arg\min_{G \in \mathbb{R}} \mathbb{E}\{e^2\} = \arg\min_{G \in \mathbb{R}} \mathbb{E}\{(\hat{y} - G\,x)^2\}$$

results in the following expression for the optimal linear gain N_x [9]

$$\begin{aligned} N_x(\sigma_x) &= \frac{\mathbb{E}\{\hat{y}\,x\}}{\sigma_x^2} \\ &= \frac{1}{\sigma_x^2} \int_{-\infty}^{+\infty} \hat{y}(x)\,x\,p(x)\mathrm{d}x \end{aligned} \qquad (2)$$

where σ_x^2 is the input signal's variance and $p(x)$ is the density function of the random variable x. Note the dependence of N_x on $\hat{y}$ in (2). This shows that the correctness of the approximating function has an essential impact on the accuracy of the corresponding DF.

A. Sinusoidal signal

An important case to consider is when x is a sinusoidal signal. The Sinusoidal Input Describing Function (SIDF) N_S can be obtained by expanding (2) into its integral form and substituting x with $A\sin(\varphi)$

$$N_S(A) = \sum_{n=0}^{R} \frac{2\alpha_n}{\pi A} \int_{-\pi/2}^{\pi/2} \left(\frac{A\,\sin(\varphi)}{\sqrt{1+A^2\sin^2(\varphi)}} \right)^{2n+1} \sin(\varphi)\,\mathrm{d}\varphi$$

where φ is considered to be uniformly distributed in the interval $[-\pi, \pi]$ such that the probability density function $p(\varphi)$ is a constant equal to $\frac{1}{2\pi}$. $N_S(A)$ can be simplified further by applying the substitution $u = \sin(\varphi)$ and taking into account that we have a perfectly odd approximation characteristic

$$N_S(A) = \sum_{n=0}^{R} \frac{4\,\alpha_n}{\pi A} \int_{0}^{1} \left(\frac{A\,u}{\sqrt{1+A^2\,u^2}} \right)^{2n+1} \frac{u}{\sqrt{1-u^2}}\,\mathrm{d}u \quad (3)$$

n	$P_E^{[n]}(A)$	$P_F^{[n]}(A)$
0	1	1
1	$A^2 + 2$	$2A^2 + 2$
2	$A^4 + \dfrac{13}{3}A^2 + \dfrac{8}{3}$	$3A^4 + \dfrac{17}{3}A^2 + \dfrac{8}{3}$
3	$A^6 + \dfrac{103}{15}A^4 + \dfrac{128}{15}A^2 + \dfrac{16}{5}$	$4A^6 + \dfrac{164}{15}A^4 + \dfrac{152}{15}A^2 + \dfrac{16}{5}$

Table 1: Polynomials belonging to (4) for n ranging between 0 and 3.

Unfortunately, no analytical solution for the integral in (3) exists. However, by using a symbolic integration package [14], the integral can be written as function of the complete elliptic integral of the first and second kind, $F(k)$ and $E(k)$ respectively

$$N_S(A) = \sum_{n=0}^{R} \frac{4\alpha_n \left(P_E^{[n]}(A)\, E(-A^2) - P_F^{[n]}(A)\, F(-A^2) \right)}{\pi A^2 (A^2 + 1)^n} \tag{4}$$

Efficient numerical implementations exist for these elliptic integrals [15]. They are readily available in most existing numerical math libraries. $P_F^{[n]}(A^2)$ and $P_E^{[n]}(A^2)$ represent even polynomials of order n in the variable A^2. These polynomials depend on the order n and can be derived by performing arithmetic manipulations on the original integral. Table 1 lists some of these polynomials [14].

B. Gaussian distributed signals

Real-world applications generally use complex modulated signals instead of pure sine waves. As an advantage, these modulated signals can be analytically approximated by white Gaussian distributed signals such that otherwise untreatable signals can still be dealt with. The method used in the sinusoidal case (using (2)) can be re-applied for retrieving the Random Input Describing Function (RIDF) $N_R(\sigma)$

$$N_R(\sigma) = \sum_{n=0}^{R} \frac{\alpha_n}{\sqrt{2\pi\sigma^3}} \int_{-\infty}^{+\infty} \left(\frac{r}{\sqrt{1+r^2}} \right)^{2n+1} r \exp\left(-\frac{r^2}{2\sigma^2} \right) dr$$

where σ is the standard deviation of the Gaussian distributed signal r. Again, a symbolic integration package [14] was used to modify the above integral into another format which includes the confluent hypergeometric function of the second kind $U(a, b, z)$ [16]

$$N_R(\sigma) = \sum_{n=0}^{R} \frac{(2n+1)!!\, \alpha_n}{2^n \sqrt{2}\sigma}\; U\left(n + \frac{1}{2},\, 0,\, \frac{1}{2\sigma^2} \right) \tag{5}$$

Here, $(n)!!$ represent the double factorial operator defined by $n(n-2)(n-4)\ldots 1$. As in the sinusoidal case, efficient numerical algorithms exist to evaluate (5) [16].

C. Verification of the obtained DFs

It is imperative to check the performance of the SIDF and RIDF, derived in Sections III-A and III-B, against the actual gain compression induced by the static nonlinear characteristic y of Fig. 1. To do so, a single-tone sine wave and a Gaussian distributed signal are applied to the system under test y and
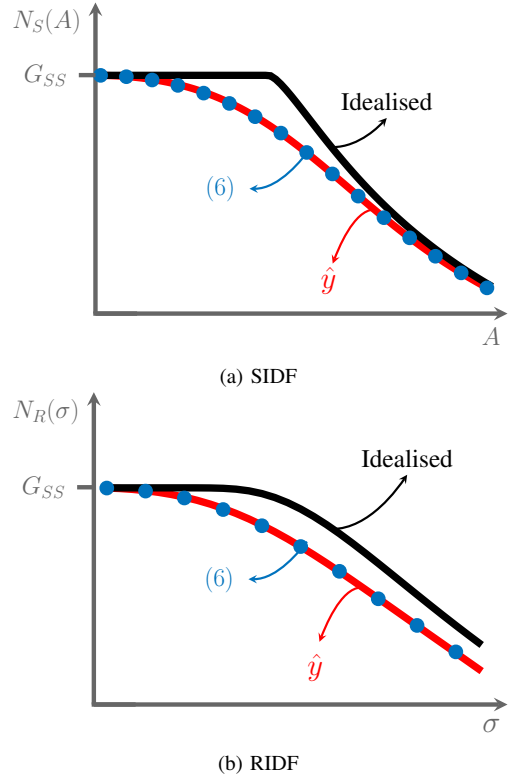
(a) SIDF

(b) RIDF

Fig. 2: In both the sinusoidal and Gaussian case the proposed approximation $\hat{y}$ ($R = 5$) outperforms the nonlinear prediction capability of the idealised one.

the large-signal linearised gain G_{LS} is derived by computing the following expression [17]

$$G_{LS}(j\omega) = \frac{S_{yx}(j\omega)}{S_{xx}(j\omega)} = \frac{\mathbb{F}\{\mathbb{E}_x\{y(t)\, x(t - \tau)\}\}}{\mathbb{F}\{\mathbb{E}_x\{x(t)x(t - \tau)\}\}} \tag{6}$$

where ω represents the angular frequency, S_{yx} is the input-output cross-power spectrum, S_{xx} is the input auto-power spectrum, $\mathbb{F}\{\bullet\}$ represents the Fourier transform and $\mathbb{E}_x\{\bullet\}$ is the expected value taken with regard to random realisations of the signal $x(t)$. In the single-tone sinusoidal case, (6) simplifies to the division of the output spectrum by the input spectrum at the excitation frequency. Also, Bussgang's theorem [18] predicts that, since we are dealing with a purely static nonlinearity, (6) becomes a constant in function of frequency for Gaussian distributed signals.

Fig. 2 shows N_S and N_R both in function of their respective input variable. To verify the performance of the DFs against the actual nonlinear behaviour, (6) has been evaluated for distinct values of A and σ. Furthermore, the obtained results were compared against the 'idealised' approximating function which is often used in existing literature (see also Fig. 1a) [9]. For low values of A and σ, the gain converges to the small-signal gain G_{SS}. Compression is visible for higher values of the input variables. The better modelling of the nonlinear characteristic provides a far better fit than the idealised one, while still being numerically efficient to compute and model. For example, evaluating (6) for a given σ on an Intel i7-4790 CPU (3.6 GHz) takes at least a minute, using 100 random realisations of the Gaussian distributed signal, while computing (5) takes less than a second.
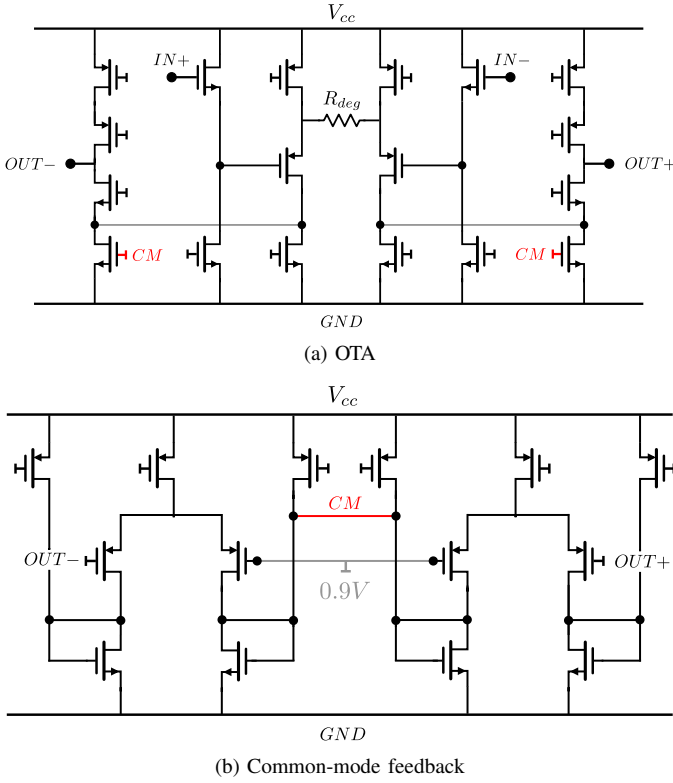
(a) OTA

(b) Common-mode feedback

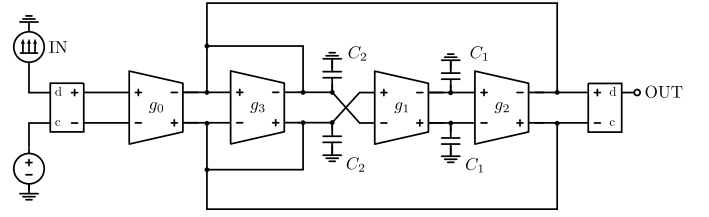Fig. 3: Circuits used during the design of the OTA.

Fig. 4: Differential Tow-Thomas biquad under study. To verify the RIDF, we excite the system with a Gaussian differential-mode multisine with varying power level.

IV. APPLICATION TO OTA-BASED CIRCUITS

The derived RIDF and SIDF are applied to a g_m-C filter and an oscillator. First, a fully differential OTA is designed in 0.18 μm CMOS (A) with a supply voltage V_{cc} equal to 1.8 V. The RIDF will thereafter be used to study the effects of a digitally modulated signal, modelled by a Gaussian MS (B), on the shape of the transfer function of a Tow-Thomas biquad filter configuration (C). The oscillator application involves the prediction of the amplitude and oscillation frequency of a quadrature OTA-based oscillator using the SIDF (D).

A. The operational transconductance amplifier

A fully differential OTA with wide bandwidth ($f_{-3dB} = 1.4$ GHz) was designed in a 0.18 μm CMOS technology. This OTA consists of three main stages (see Fig. 3a):

- An input stage which level shifts the input common-mode voltage from 0.9 V to 0.4 V via two source followers. By doing so, the large-signal handling capability of the OTA is significantly increased.
- The transconductance stage which provides most of the g_m needed for the voltage to current conversion. Source degeneration (R_{deg}) has been included to linearise the response of the OTA.
- An output stage which delivers the high output impedance via a folded cascode configuration.

The common-mode voltage at the output nodes is stabilised at 0.9 V, i.e. half of the power supply V_{cc}, by an active common-mode circuit (see Fig. 3b).

Every practical OTA exhibits nonlinear saturation effects which limit the obtainable dynamic range. The static voltage-to-current relationship can be constructed to evaluate the behaviour and severeness of this saturation phenomenon. In the case of the OTA this boils down to performing a DC sweep of the differential input voltage and examining the corresponding differential current which flows through a shorted output. This voltage-current relationship is actually the one that has been used as an example in Section III (x and y are the voltage and the current respectively), which means that the SIDF and RIDF for this specific OTA were already illustrated in Fig. 2. G_{SS} of the OTA is equal to 625 μS.

B. Multisines as realistic excitation signal

Obtaining a good match between simulation and reality does not only require accurate device models. Equally important are the excitation signals which are considered during the design phase [8]. As it turns out, most applications do not expect single-tone excitations or Gaussian distributed signals during their real-world operation. For example, wireless telecommunication systems apply their complex digital modulation in a pre-specified frequency band which results in an approximately flat power spectrum.

Multisines (MS) consist of several simultaneously generated sinusoidal tones, which can be described mathematically by

$$x(t) = \sum_{r=1}^{F} A_r \sin(2\pi r f_0 t + \varphi_r) \tag{7}$$

where A_r and φ_r are, respectively, the amplitude and phase of the rth spectral line of the MS excitation and f_0 the frequency resolution. F is the number of tones present in the MS signal.

Random-phase multisines are signals which can simulate any user-defined amplitude spectrum, while conserving properties like periodicity of the signal and Gaussianity of the probability density function. These properties make them well suited for very efficient simulation of systems while preventing drawbacks in the frequency domain transformation, such as leakage and possible aliasing, that are related to random variables [19]. The Gaussianity property can be easily obtained by choosing φ_r uniformly in the interval $[0, 2\pi[$ and $F \to \infty$. By doing so, results from the RIDF can be directly applied to this MS excitation such that they can effectively replace white Gaussian noise for simulation purposes.

$$\sigma_k^2 \leftarrow \sigma_{IN}^2$$
$$\vec{g} \leftarrow N_R(\sigma_{IN}) \text{ using (5)}$$
do

    $\vec{g}_{old} \leftarrow \vec{g}$

    % Compute all the transfer functions with $\vec{g}$
    $H_k(s, \vec{g}) \leftarrow T_{IN \to k}(s, \vec{g})$

    for every node k **do**

        $\sigma_k^2 \leftarrow$ evaluate (9) or (10)
        $\vec{g}_k \leftarrow N_R(\sigma_k)$ defined in (5)

    end for

while $\max\{|(\vec{g} - \vec{g}_{old}) ./ \vec{g}|\} <$ max relative error

Alg. 1: Iterative algorithm for the derivation of the correct σ_k^2 and the corresponding transconductance vector $\vec{g}$. The termination condition of the algorithm is based on the relative variation of each of the transconductances. $T_{IN \to k}(s, \vec{g})$ represents the transfer function from the input to node k, $\vec{g}_k$ is the subset of all transconductances which depend on σ_k and $./$ is the element-wise vector division operator.

C. g_m-C Tow-Thomas biquad

Early research [20] has shown that any transfer function needed for active filter design can be established by the exclusive use of OTAs and capacitors, laying the foundation for g_m-C filters. One widely used method to realise high-order filters is by cascading second-order g_m-C biquads. A popular biquad is the so-called Tow-Thomas biquad (see Fig. 4). This specific g_m-C architecture consists of two integrators, one ideal and one lossy, connected in a feedback configuration [21].

The biquad exhibits the following differential low-pass transfer function $T(s, \vec{g})$ from input to output voltage

$$T(s, \vec{g}) = \frac{-g_0 \, g_1}{C_1 \, C_2 \, s^2 + g_3 \, C_1 \, s + g_1 \, g_2} \quad (8)$$

where s is the complex Laplace variable, g_1-g_4 and C_1-C_2 are, respectively, the transconductances of the OTAs and the capacitors present in Fig. 4. $\vec{g}$ represents the vector of all tranconductances combined, i.e. $\vec{g} = (g_1, g_2, g_3, g_4)$.

A straightforward method to evaluate the effectiveness of the obtained RIDF would be to plug it in (8) and look at the changes for varying σ. However, this approach is fundamentally wrong, the reason being that each of the OTAs has a different σ at its respective input which should be taken into account. Looking at the existing literature, single feedback systems containing multiple nonlinearities were only investigated for sinusoidal signals due to their easy graphical interpretation [9], [22].

To take these multiple nonlinear OTAs into account for Gaussian distributed signals, we start from the input power level σ_{IN}^2 and use linear system theory to retrieve an estimate of the power σ_k^2 at every node k present in the network. The following relationship can be used for the derivation of σ_k^2 [9]

$$\sigma_k^2 = \frac{1}{f_s/2} \int_0^{f_s/2} \Phi_{IN}(j2\pi f) \, |H_k(j2\pi f, \vec{g})|^2 \, df \quad (9)$$

where f_s represents the sampling frequency, Φ_{in} is the input power spectral density and $H_k(j2\pi f, \vec{g})$ is the linear symbolic
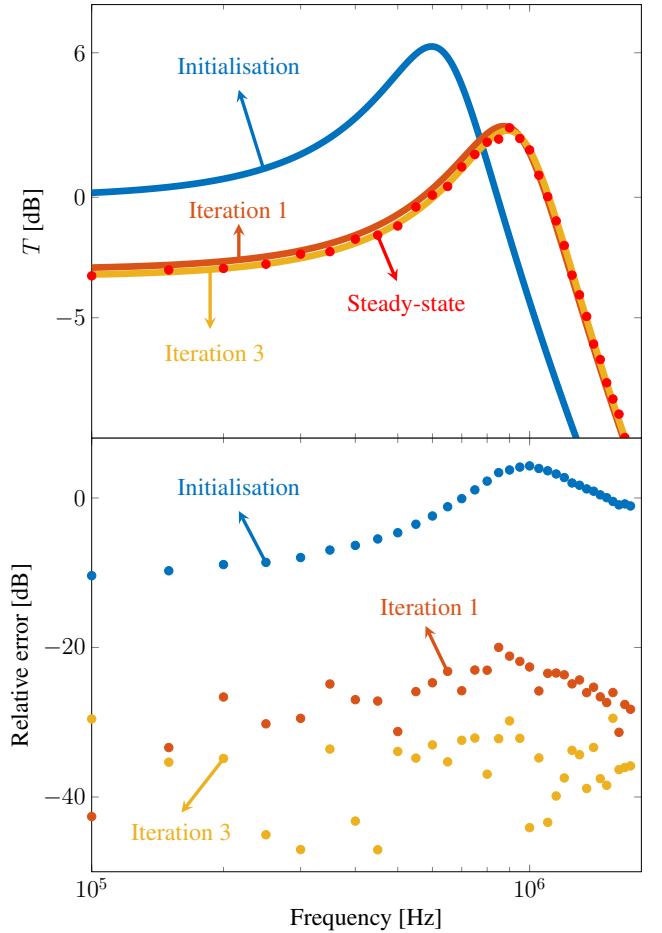

Fig. 5: Different iterations of Alg. 1 show that the proposed algorithm converges rapidly (only 3 iterations are needed) to acquire a good estimate of the actual behaviour obtained through a steady-state analysis ($\sigma_{IN} = 0.3 \, V_{RMS}$).

transfer function from the input to node k. Equation (9) can be further simplified if we consider that the input signal is white Gaussian noise modelled by random phase multisines (see (7))

$$\sigma_k^2 = \frac{\sigma_{IN}^2}{F} \sum_{r=1}^{F} |H_k(j2\pi \, r f_0, \vec{g})|^2 \quad (10)$$

where σ_{IN}^2 is the power of the input signal.

The transfer functions $H_k(s, \vec{g})$ can be derived using the modified nodal analysis on the equivalent linear circuit [23]. This equivalent circuit is obtained by replacing the OTAs with an ideal voltage-controlled current source. Symbolic circuit analysis tools exist (e.g. [24]) which allow to automatically generate $H_k(s, \vec{g})$.

These linear symbolic transfer functions are indirectly dependent on σ_k^2 through $\vec{g}$, which means that (9) cannot be solved directly. To cope with this issue, we propose to use an iterative scheme which can deal with this dependence (see Alg. 1). Since Alg. 1 is a nonlinear optimisation scheme, potential convergence issues could arise. As it turns out, no convergence problems were encountered in all considered cases. One possible method to mitigate convergence issues, when encountered, is to improve the estimates of σ_k^2 during the initialisation by performing an AC analysis on the circuit and subsequently calculating (10).
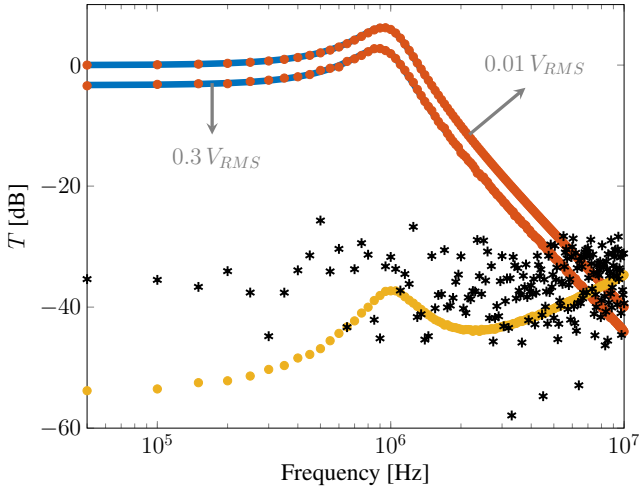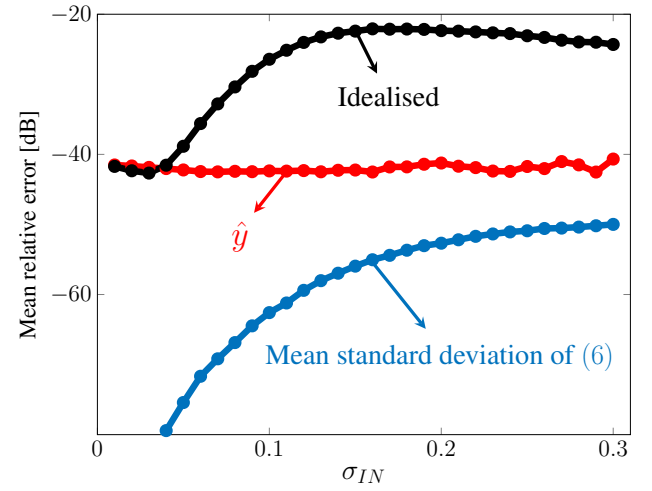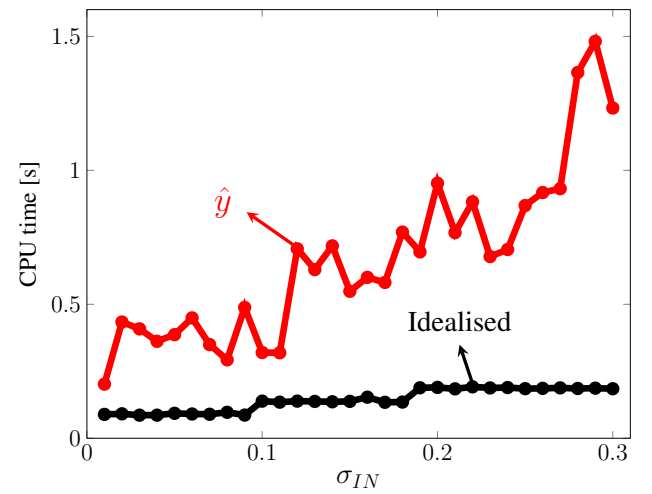
(a) Proposed RIDF from (5)
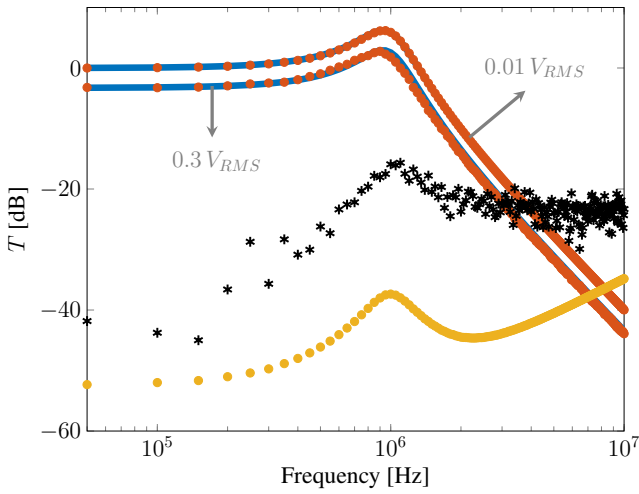
(b) Idealised RIDF

Fig. 6: The transfer function T of the biquad changes when the input RMS value is increased from $0.01\,V_{RMS}$ to $0.3\,V_{RMS}$. $-$: TF predicted with the RIDF, •: simulation results from harmonic balance, •: relative error for $\sigma_{IN} = 0.01\,V_{RMS}$ and $*$: relative error for $\sigma_{IN} = 0.3\,V_{RMS}$.

(a) Mean relative error

(b) CPU time

Fig. 7: Comparison of the mean relative error (a) and CPU time (b) for the proposed and idealised RIDF in function of σ_{IN}. Additionally, the standard deviation resulting from the estimation in (6) is shown for 200 different random phase realisations.

The iterative procedure of Alg. 1 is applied to the Tow-Thomas biquad example (see fig. 4). The capacitors and transconductances are chosen such that a quality factor of 2 and a resonance frequency of $1\,MHz$ are obtained. By varying the Root-Mean Square (RMS) value of the input Gaussian MS excitation from $0.01\,V_{RMS}$ to $0.3\,V_{RMS}$, the prediction capability of the proposed scheme can be verified against simulation results obtained with a transistor-level harmonic balance analysis and evaluation of (6). The Gaussian MS used here has a frequency resolution f_0 of $50\,kHz$ and contains 200 excited tones.

To verify the performance of the proposed iterative scheme, different iterations of Alg. 1 have been showcased in Fig. 5 for $\sigma_{IN} = 0.3\,V_{RMS}$. The initialisation of the transfer function used shows that not using the proposed Alg. 1 would result in a big discrepancy between the actual behaviour and the idealised behaviour obtained by the idealised DF analysis. In the case of the biquad only 3 iterations of the algorithm were needed to obtain a good approximation of the steady-state analysis

(an undeterministic relative error fluctuating around -35 dB is obtained). More iterations are needed when more complex transfer functions are involved. For example, increasing the Q-factor of $T(s, \vec{g})$ in (8) from 2 to 4 already required on average one more iteration.

Fig. 6 shows the influence of an increase of input RMS value on the transfer function $T(s)$ of the biquad, and this for both the proposed and the idealised approximation. The following observations can be made

• Increasing σ_{IN} does not exclusively result in gain compression. It also alters the resonance frequency of the biquad (only slightly visible in the figure).
• Both RIDFs exhibit the same behaviour at low σ_{IN}, as is shown by the equal relative error •.
• The relative error in the case of the idealised RIDF at $0.3\,V_{RMS}$ shows an increased deterministic dynamic behaviour close to the resonance frequency. This indicates that the idealised RIDF does not well model the change in resonance frequency.

To further analyse the capabilities of both RIDFs, we compared the accuracy (relative error) and efficiency (simulation time) in function of σ_{IN} (see Fig. 7). The mean of the relative error over frequency has been chosen to represent the accuracy such that for each σ_{IN} a single figure of merit could be extracted. Again, the results obtained with Alg. 1 were verified against transistor-level harmonic balance simulations. The average simulation time for one realisation of (6) with a Gaussian MS excitation was 1,34 seconds on the same machine. Unfortunately, the quality of the estimate when using Gaussian MS excitations is distorted by nonlinear effects which result in an increased variability of the relative error (see Fig. 6). Enough realisations should be considered for (6) to guarantee that the relative error is a measure for the prediction capabilities of the RIDF and is not dominated by the adverse effects of nonlinear distortions on the estimate. For our application, 200 different realisations were needed to ensure that the mean standard deviation of (6) for all considered σ_{IN} was well below every mean relative error (minimum 10 dB in our case) such that errors introduced by the RIDF could be detected. This standard deviation scales with the square root law and is dependent on σ_{IN} (see Fig. 7a).

Analyzing Fig. 7a shows that the proposed RIDF is characterised by an approximately constant relative error (-40 dB) in function of σ_{IN}. This is not the case for the idealised RIDF where the mean relative error rises to a maximum value of -22 dB. However, this increase in accuracy is coupled with a small loss in computational efficiency (see Fig. 7b). Investigation of Fig. 7b shows that the CPU time is not constant in function of σ_{IN}:

- The idealised RIDF shows two jumps in the computation time which correspond with an increment of the iteration count in Alg. 1.
- These jumps in iteration count are less apparent for the proposed RIDF. This behaviour is caused by the numerical evaluation of (5) for which the computation time depends on the input parameters of $U(a, b, z)$ [25].

The idealised RIDF takes utmost $0.19 \, s$ to solve Alg. 1 while the proposed RIDF has to compute maximally for $1.5 \, s$. These computation times are still significantly lower than the harmonic balance simulation time with 200 realisations, which takes 4 minutes and 28 seconds for a single σ_{IN}.

From the above comparisons, we can conclude that the proposed RIDF exhibits a much lower relative error than the idealised RIDF while still being efficiently computable.

D. Quadrature OTA-based oscillator

On-chip automatic tuning is essential to avoid that parasitic phenomena such as thermal variations, parasitic capacitances, fabrication tolerances and mismatches influence the envisioned performance. A generally adopted choice by CMOS filter designers is the master-slave tuning system which employs a Phase-Locked Loop (PLL) as master to generate a proper tuning signal for the slave system [26], [27]. The core of this PLL is a voltage-controlled oscillator which should be carefully matched to the slave system.
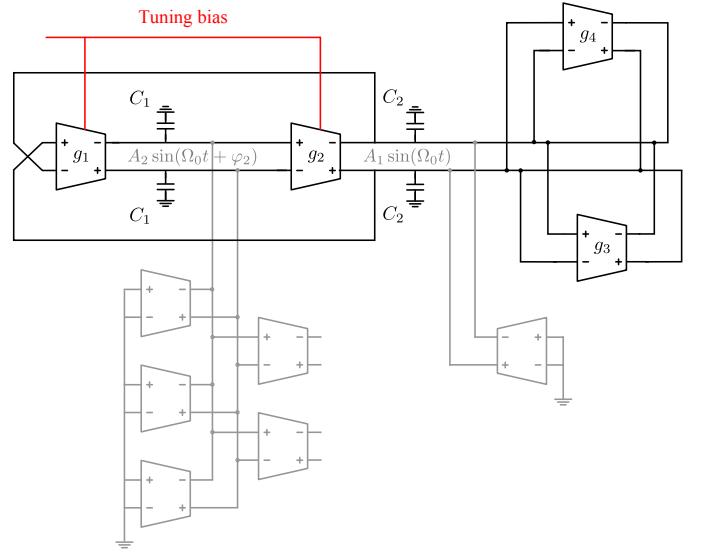

Fig. 8: Differential quadrature oscillator under study. Dummy OTAs are added (gray) such that each node of the oscillator sees the same parasitic capacitance and output conductance. The SIDF presumes perfect sinusoidal operation at a certain angular frequency Ω_0.

Keeping the above mentioned application in mind, we want to verify how well the derived SIDF can predict the oscillation amplitude and frequency of a sinusoidal g_m-C oscillator. Consider for this purpose the quadrature oscillator depicted in Fig. 8 [10]. It consist of two parts: a linear part which sets the oscillation frequency (g_1, g_2, C_1 and C_2), and a nonlinear part which ensures start-up and stabilises the amplitude (g_3 and g_4). The poles of such a quadrature oscillator can be generally described by the following characteristic equation

$$s^2 - b\,s + \Omega_0^2 = 0 \tag{11}$$

where b represents the boundary conditions of the oscillation and Ω_0 sets the oscillation frequency.

Both b and Ω_0 are a function of the transconductances g_i, the total capacitances ($C_i^{tot} = C_i + 3\,C_{in} + 4\,C_{out}$) and the total output conductances ($g_{o1}^{tot} = g_{o1} + 3\,g_o^{dummy}$ and $g_{o2}^{tot} = g_{o2} + g_{o3} + g_{o4} + g_o^{dummy}$) that are present in the circuit [28]

$$b = \frac{(g_4(A_1) - g_3(A_1) - g_{o2}^{tot}(j\Omega_0))\,C_1^{tot} - g_1^{tot}(A_1)\,C_2^{tot}}{C_1^{tot}\,C_2^{tot}} \tag{12}$$

$$\begin{aligned} \Omega_0^2 &= \frac{g_1(A_1)\,g_2(A_2)}{C_1^{tot}\,C_2^{tot}} \\ &+ \frac{g_{o1}^{tot}(j\Omega_0)\,(g_4(A_1) - g_3(A_1) + g_{o2}^{tot}(j\Omega_0))}{C_1^{tot}\,C_2^{tot}} \end{aligned} \tag{13}$$

Herein, A_1 and A_2 represent the magnitudes of the differential input sinusoid of the nonlinearity (see Fig. 8). Ω_0 is the angular frequency at which the oscillation is running. Similarly to the previous example, we define $\vec{A}$ as the vector which contains all the amplitudes of the single-tone sinusoid for the different nodes in the circuit, i.e. $\vec{A} = (A_1, A_2)$. To avoid the presence of an asymmetry in the oscillator, dummy OTAs where added in

$A_1 \leftarrow$ fixed value
$\Omega_0 \leftarrow 0$
do

    $\Omega_{old} \leftarrow \Omega_0$
    % Compute all other amplitudes A_k recursively
    % starting from A_1
    for every node k **do**

        $A_{k+1} \leftarrow |T_{k \to k+1}(j\Omega_0)| \, N_S^k(A_k) \, A_k$

    end for

    $\Omega_0 \leftarrow$ evaluate (13) using $\vec{A}$ and Ω_0

while $|(\Omega_0 - \Omega_{old}) / \Omega_0| <$ max relative error
$b(A_1) \leftarrow$ evaluate (12) with derived Ω_0 and $\vec{A}$

Alg. 2: Iterative scheme for the derivation of b and Ω_0 in function of A_1. The termination condition is based on the relative variation of the oscillation frequency. $T_{k \to k+1}(j\Omega_0)$ represents the linear transfer function from node k to node $k+1$, while $N_S^k(A_k)$ is the SIDF of the nonlinear element in between node k and $k+1$.

Fig. 8 to ensure that every respective differential node is loaded by the same parasitic capacitance and output conductance.

An ideal oscillator would not include the coefficient b (purely imaginary poles). However, due to finite output impedance of the OTAs, a mechanism has to be put in place to compensate for the losses of this non-ideality and allow self-startup of the oscillation. The nonlinear behaviour of g_3 and g_4 with regard to A_1 has been constructed in such a way (by choosing a proper R_{deg} in Fig. 3a) that g_4 is larger than g_3 but g_4 also starts to compress earlier. In this way, self-startup is ensured [10] and the initially unstable poles will converge to the imaginary axis with a certain amplitude vector $\vec{A_0}$.

A pertinent question remains still unsolved: how can we deduce the steady-state oscillation parameters $\vec{A_0}$ and Ω_0 using the SIDF? The solution uses the observation that the characteristic equation (11) only reaches steady state if b equals to 0. Thus, by solving (12) as a function of the vector $\vec{A}$, and using the SIDF ($g_i(A_k) = N_S(A_k)$), we can deduce at which amplitudes $b(\vec{A})$ crosses the zero-axis. If the slope of b at these possible multiple intersections is negative, then the obtained oscillation can be proven to be stable and unique [22].

Although the general approach has been explained in the previous paragraph, two issues still need to be figured out before applying the method:

- The amplitudes in $\vec{A}$ are not independent from each other. By fixing one arbitrary amplitude A_k, all the others can be derived via the closed-loop linearised transfer function from node k to the node under consideration. This requires to replace the nonlinear systems with their respective SIDF N_S [22].
- The OTA is not a purely static nonlinear system. If this would be the case, the derivation of Ω_0 would be greatly simplified: the output conductance would be a frequency-independent constant in that case. However, this would adversely impact the estimation accuracy of the oscillation frequency. To take the frequency dependence of the output conductance of the OTA into account, we need to solve
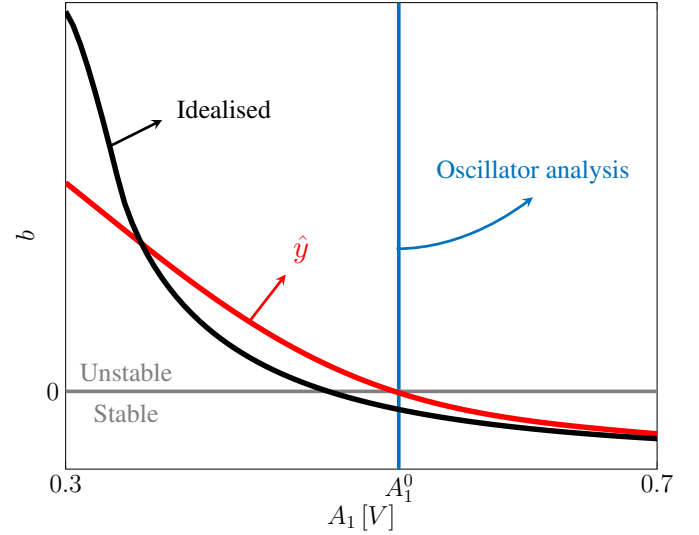
(a) b in function of A_1. The zero-crossing with the x-axis predicts at which amplitude the oscillation will take place.
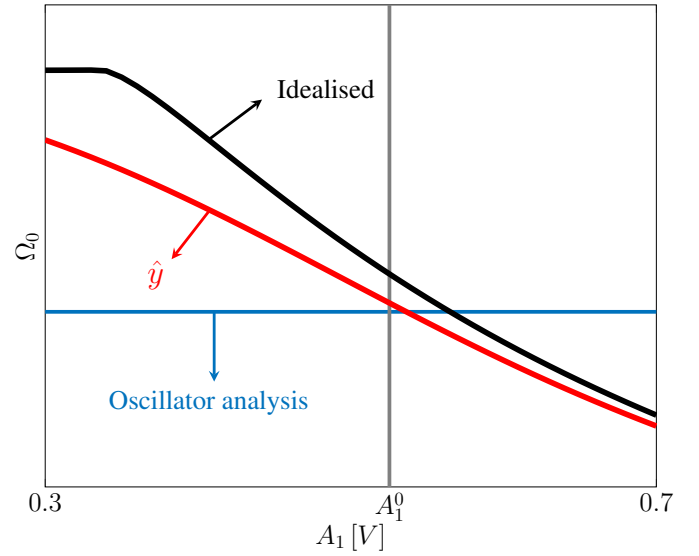
(b) Ω_0 in function of A_1.

Fig. 9: Comparing the idealised and proposed approximation, $\hat{y}$ provides a better estimation of the steady-state oscillation amplitude and frequency.

an implicit equation (see (13)). Again, we propose to use an algorithm which iteratively copes with this frequency dependence (see Alg. 2).

This iterative scheme is implemented and applied to the previously introduced quadrature oscillator. The capacitances and transconductances are chosen such that an oscillation frequency of around $1\,\text{MHz}$ is obtained. Fig. 9 shows the resulting b and Ω_0 in function of A_1 which required 3 iterations of Alg. 2. To provide a comparison, the analysis has been applied to both the idealised and proposed SIDF.

As a first step, the steady-state oscillation amplitude A_1^0 is deduced from Fig. 9a by determining where b crosses the zero-axis. If we compare this value to the one retrieved with an oscillator analysis, we can conclude that the idealised SIDF significantly underestimates the real amplitude (see Table 2). However, the proposed N_S (3) results in an amplitude which

Method	Relative error A_0	Relative error Ω_0	CPU time
Oscillator analysis	-	-	$5.29\,s$
Proposed SIDF	-45.1 dB	-34.6 dB	$0.70\,s$
Idealised SIDF	-20.8 dB	-16.9 dB	$0.64\,s$

Table 2: Comparison of the different techniques.

almost coincides (relative error of -45.1 dB) with the one predicted by the oscillator analysis.

Knowing the correct amplitude A_1^0, we can now deduce the oscillation frequency which is predicted by the SIDF. Fig. 9b shows that both SIDFs overestimate the oscillation frequency even if the correct amplitude is used. However, the prediction for $\hat{y}$ is more accurate than the idealised one (see Table 2). This overestimation can be explained by observing that the definition of the SIDF (2) does not take into account the phase shift that is caused by the dynamic behaviour of the OTA. It exclusively looks at the gain compression. Since the oscillation frequency is influenced by phase shifts present in the feedback loop, this results in a model error as the SIDF cannot model these effects.

Analyzing the computation times in Table 2 shows that using the proposed SIDF does not significantly increase the computational cost compared to the idealised one. Furthermore, both SIDFs are computationally more efficient than performing an oscillator analysis using the Advanced Design System (ADS) software of Keysight.

Simulations have shown that the prediction capability of the DF approach declines with increasing oscillation amplitude. This behaviour is caused by growing harmonics which are no longer negligible compared to the fundamental tone. One possible method to verify the validity of the DF approach is to calculate the Higher-Order SInusoidal Describing Functions (HOSIDF) of the proposed approximating function [29]. These HOSIDF derive an amplitude dependent gain for the harmonic components generated by the static nonlinearity. Using these HOSIDF, the amplitude level at which the harmonic content becomes too dominant could be derived such that the validity of the DF approach could be investigated. However, this derivation will be the subject of future research.

V. CONCLUSION

The Describing Function model introduced in this paper allows to accurately predict the nonlinear behaviour of devices which exhibit saturation phenomena. Its main advantage is that the DF can be directly fitted starting from the saturation characteristic. This eliminates the need to make assumptions about the shape of the saturation behaviour. As it turns out, the proposed DF for sinusoidal signals and Gaussian distributed signals can be efficiently computed numerically.

The improved DF has been demonstrated on a g_m-C Tow-Thomas filter and a quadrature oscillator. In both cases, an iterative scheme was developed which allows the use of the DF in a practical design. Moreover, it was shown that the proposed DF outperforms the DF of the idealised saturation function which is often used in existing literature.

REFERENCES

[1] E. Sanchez-Sinencio and J. Silva-Martinez, "CMOS transconductance amplifiers, architectures and active filters: a tutorial," *IEEE proceedings-circuits, devices and systems*, vol. 147, no. 1, pp. 3–12, 2000.

[2] B. Linares-Barranco, A. Rodriguez-Vazquez, E. Sanchez-Sinencio, and J. Huertas, "CMOS OTA-C high-frequency sinusoidal oscillators," *IEEE Journal of solid-state circuits*, vol. 26, no. 2, pp. 160–165, 1991.

[3] A. D. Grasso, D. Marano, G. Palumbo, and S. Pennisi, "Design Methodology of Subthreshold Three-Stage CMOS OTAs Suitable for Ultra-Low-Power Low-Area and High Driving Capability," *IEEE Transactions on Circuits and Systems I: Regular Papers*, vol. 62, no. 6, pp. 1453–1462, 2015.

[4] O. Abdelfattah, G. W. Roberts, I. Shih, and Y.-C. Shih, "An Ultra-Low-Voltage CMOS Process-Insensitive Self-Biased OTA With Rail-to-Rail Input Range," *IEEE Transactions on Circuits and Systems I: Regular Papers*, vol. 62, no. 10, pp. 2380–2390, 2015.

[5] S. Szczepanski and R. Schaumann, "Nonlinearity-induced distortion of the transfer function shape in high-order OTA-C filters," *Analog Integrated Circuits and Signal Processing*, vol. 3, no. 2, pp. 143–151, 1993.

[6] J. F. Fernandez-Bootello, M. Delgado-Restituto, and Á. Rodríguez-Vázquez, "Matrix methods for the dynamic range optimization of continuous-time-filters," *IEEE Transactions on Circuits and Systems I: Regular Papers*, vol. 55, no. 9, pp. 2525–2538, 2008.

[7] P. Wambacq and W. Sansen, *Distortion analysis of analog integrated circuits*, vol. 451. Springer Science & Business Media, 2013.

[8] L. De Locht, Y. Rolain, and G. Vandersteen, "Designing power amplifiers? Use good excitation signals," in *ARFTG Conference, 2006 67th*, pp. 211–213, IEEE, 2006.

[9] A. Gelb and W. Vander Velde, *Multiple-input describing functions and nonlinear system design*. New York: McGraw-Hill, 1968.

[10] J. Kardontchik, "Introduction to the design of transconductor-capacitor filters," *Boston: Kluwer Academic Publishers*, vol. 1, p. 992, 1992.

[11] P. R. Gray and R. G. Meyer, *Analysis and design of analog integrated circuits*. John Wiley & Sons, Inc., 1990.

[12] K. Kimura, "The ultra-multi-tanh technique for bipolar linear transconductance amplifiers," *IEEE Transactions on Circuits and Systems I: Fundamental Theory and Applications*, vol. 44, no. 4, pp. 288–302, 1997.

[13] C. D. Salthouse and R. Sarpeshkar, "Jump resonance: a feedback viewpoint and adaptive circuit solution for low-power active analog filters," *IEEE Transactions on Circuits and Systems I: Regular Papers*, vol. 53, no. 8, pp. 1712–1725, 2006.

[14] I. Wolfram Research, "Wolfram alpha."

[15] B. C. Carlson, "Numerical computation of real or complex elliptic integrals," *Numerical Algorithms*, vol. 10, no. 1, pp. 13–26, 1995.

[16] L. J. Slater, *Confluent hypergeometric functions*. University Press Cambridge, 1960.

[17] R. Pintelon and J. Schoukens, "FRF measurement of nonlinear systems operating in closed loop," *Instrumentation and Measurement, IEEE Transactions on*, vol. 62, no. 5, pp. 1334–1345, 2013.

[18] J. Bussgang, "Cross-correlation functions of amplitude-distorted gaussian inputs," *Nonlinear systems. Stroudsburg, PA: Dowdon, Hutchinson & Ross*, 1975.

[19] R. Pintelon and J. Schoukens, *System identification: a frequency domain approach*. John Wiley & Sons, 2012.

[20] M. Bialko and R. Newcomb, "Generation of all finite linear circuits using the integrated DVCCS," *IEEE Transactions on Circuit Theory*, vol. 18, no. 6, pp. 733–736, 1971.

[21] Y. Sun, *Design of high frequency integrated analogue filters*. No. 14, Iet, 2002.

[22] E. Davison and D. Constantinescu, "A describing function technique for multiple nonlinearities in a single-loop feedback system," *IEEE Transactions on Automatic Control*, vol. 16, no. 1, pp. 56–60, 1971.

[23] G. Gielen and W. Sansen, *Symbolic analysis for automated design of analog integrated circuits*, vol. 137. Springer Science & Business Media, 2012.

[24] A. Montagne, "SLiCAP - Symbolic Linear Circuit Analysis Program."

[25] J. W. Pearson, S. Olver, and M. A. Porter, "Numerical methods for the computation of the confluent and gauss hypergeometric functions," *Numerical Algorithms*, pp. 1–46, 2016.

[26] F. Krummenacher and N. Joehl, "A 4-MHz CMOS continuous-time filter with on-chip automatic tuning," *IEEE Journal of Solid-State Circuits*, vol. 23, no. 3, pp. 750–758, 1988.

[27] R. Schaumann and M. A. Tan, "The problem of on-chip automatic tuning in continuous-time integrated filters," in *Circuits and Systems, 1989., IEEE International Symposium on*, pp. 106–109, IEEE, 1989.

[28] J. Galan, R. G. Carvajal, A. Torralba, F. Munoz, and J. Ramirez-Angulo, "A low-power low-voltage OTA-C sinusoidal oscillator with a large tuning range," *IEEE Transactions on Circuits and Systems I: Regular Papers*, vol. 52, no. 2, pp. 283–291, 2005.

[29] P. Nuij, O. Bosgra, and M. Steinbuch, "Higher-order sinusoidal input describing functions for the analysis of non-linear systems with harmonic responses," *Mechanical Systems and Signal Processing*, vol. 20, no. 8, pp. 1883–1904, 2006.

Gerd Vandersteen (1968, Belgium) received the degree in electrical engineering in 1991 and his PhD in electrical engineering in 1997, both from the VUB, Brussels, Belgium. He was with the Micro-Electronics Research Centre IMEC, Wireless Group, as a Principal Scientist, with a focus on modeling, measurement, and simulation of electronic circuits in state-of-the-art silicon technologies. This research was in the context of a collaboration with the VUB. Since 2008, he has been a Professor with the Department of Fundamental Electricity and Instrumentation, VUB, within the context of measuring, modelling and analysis of complex linear and nonlinear system. Within this context, the set of systems under consideration is extended from micro-electronic circuits towards all kinds of electro-mechanical systems. Since 2011, he has been the director of the Doctoral School of Natural Sciences and (Bioscience) Engineering (NSE), VUB.

Dries Peumans (1992, Belgium) graduated as an Engineer in Electronics and Information Technology in 2015 at the VUB. Afterwards he joined the department ELEC as a PhD researcher. His research focuses on nonlinear modelling and the design of analog circuits.